Surface scientific aspects in semiconductor electrochemistry

H. J. Lewerenz†

Brandenburgische Technische Universität Cottbus, Faculty of Physics, Erich-Weinert-Str. 1, 03046 Cottbus, Germany

CHEMICAL SOCIETY REVIEWS

Some of the fundamental properties of the reactive semiconductor–electrolyte interface are outlined and possibilities for electrochemical modification of semiconductor surfaces are discussed. The present status of investigating the physicochemical and morphological changes after (photo-electrochemical) processing is reviewed for selected examples. The accessibility of near surface changes by a selection of surface sensitive techniques is presented and the information obtained by ultrahigh vacuum *ex situ* methods such as high resolution electron energy loss spectroscopy (HREELS), and ultraviolet photoelectron spectroscopy (UPS) is compared with *in situ* techniques such as Fourier transform infrared spectroscopy (FTIR). The suitability of electrochemistry–atomic force microscopy (EC–AFM) to follow *in situ* the surface microtopographic changes during electrochemical processes is emphasised. Examples are presented on the electrochemically hydrogenated Si (111) surface and on monitoring *in situ* the changes at the silicon–silicon oxide–electrolyte interfacial region during current oscillations.

1 Introduction

The continuous improvement of investigative methods over the last 15 years has resulted in a wealth of new possibilities to extract information on interfacial changes at semiconductors subjected to electrochemical or photoelectrochemical treatment.[1–5] As a consequence, the field is characterized by the technical development of the analysis methods and simultaneously by the advances in reproducible electrochemical surface conditioning.[6–8] Many of the advances stem from purely fundamental research but frequently applications could be found. Among such examples are the electrochemical hydrogenation of silicon which occurred in the course of a still rather obscure current transient,[3,5,6] smoothing of Si due to current oscillations,[9] photoelectrochemical surface transformation of InP and $CuInSe_2$ in electrochemical solar cells[10,11] and photoelectrochemical etching of layered materials for solar cell application,[12] for instance.

There are, of course, many other results and applications but in this article I will restrict myself to examples which represent the technical advancement and diversity of the analysis methods employed and to specific recent selected results on electrochemical semiconductor surface alteration. As an overview, Fig. 1 shows some of the areas of possible applications of semiconductor electrochemistry.

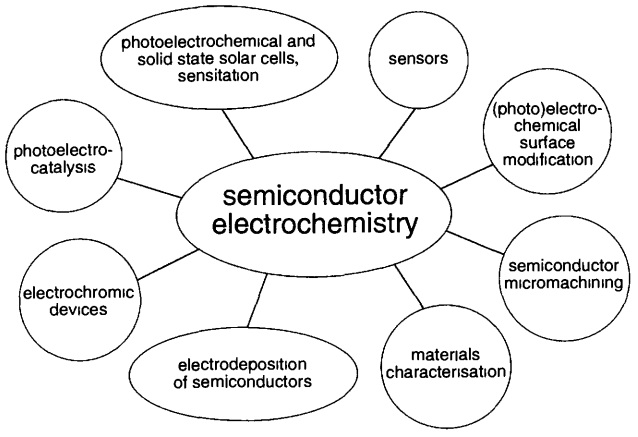

Fig. 1 Schematic on applications of semiconductor electrochemistry

In sensors, for instance, the potential and current control which is typical for electrochemical processing can improve the selectivity of the species to be detected; solid state or photoelectrochemical solar cells can be improved by surface modifications which result in improved electronic properties and/or interfacial layers which inhibit or suppress leakage currents or chemical reactions with ambient or contact phases.[13,14] In micromechanics, the extended application of electrochemical processing, particularly of Si, would allow high reproducibility of very well-ordered structures. Other important areas are electrodeposition of semiconducting films,[15] light-induced electrocatalysis[16] and the characterization of the basic semiconductor properties following film preparation in a materials development laboratory.

Hans-Joachim Lewerenz studied physics at the Technical University Berlin, and obtained MS and PhD thesis at the Fritz-Haber Institut der Max Planck-Gesellschaft on photoemission from metals into electrolytes. He was a member of the technical staff for two postdoctoral years at Bell Laboratories, Murray Hill, working on semiconductor and photoelectrochemical interfaces, and photoelectrochemical solar cells. As a member of staff at the Brown Boveri Research Center in Switzerland, his research area was catalysis. He has worked at the Hahn-Meitner-Institute since 1982, conducting research on photovoltaics, semiconductor materials science and photoelectrochemistry. He has been an honorary Professor of Physics at the Technical University of Berlin since 1993, and is a visiting professor at the Technical University Cottbus (1996/97). He is currently head of the department of interfaces at the Hahn-Meitner-Institute. He has published over 140 scientific articles and a book on photovoltaics, and holds 13 patents.

† *Permanent address*: Hahn-Meitner-Institut Berlin GmbH, Glienicker Str. 100, 14109 Berlin, Germany.

2 The reactive surface

In comparison to surfaces exposed and investigated in an ultrahigh vacuum (UHV) environment, where the preparation of the solid surface itself is often problematic, the surface of a semiconductor 'forms' upon immersion into the respective electrolyte. Electrochemical parameters can influence the surface conditions *via* potential and current flow and subsequently lead to alterations due to the interfacial reactivity.

A view of the surface region is given in Fig. 2. Fig. 2(*a–b*) show the surface and interface properties on a more microscopic scale, whereas Fig. 2(*c*) displays some of the mesoscopic features. In concentrated electrolytes and not too highly doped semiconductors, the Galvani potential drop appears predominantly on the semiconductor side, since the respective capacitances C_{HH} (outer Helmholtz layer) and C_{SC} (space charge layer) can differ by a factor of *ca.* 100, depending on relative permittivities in the semiconductor and the Helmholtz layer and on the doping level as well as on ionic concentration in solution. Thus, the relative voltage drop is determined from eqn. (1).

$$\frac{Q}{C_t} = Q\left(\frac{1}{C_{HH}} + \frac{1}{C_{SC}}\right) \tag{1}$$

It is almost negligible on the electrolyte side (C_t total capacitance). Applied potentials drop predominantly in the semiconductor surface and space charge region, allowing the investigation of the semiconductor using potential and current as parameters. The inner Helmholtz layer, characterized by the centre of specifically adsorbed ions is already an example for the reactivity of the surface. Defining the point of zero charge (pzc) as the potential at which ideally no excess charge exists on both sides of the junction (characterized experimentally by a minimum in the differential capacitance[17] one observes for instance adsorption of anions negative from the pzc. This behaviour is attributed to the chemical reactivity of the semiconductor with a specific ion in solution which is strong

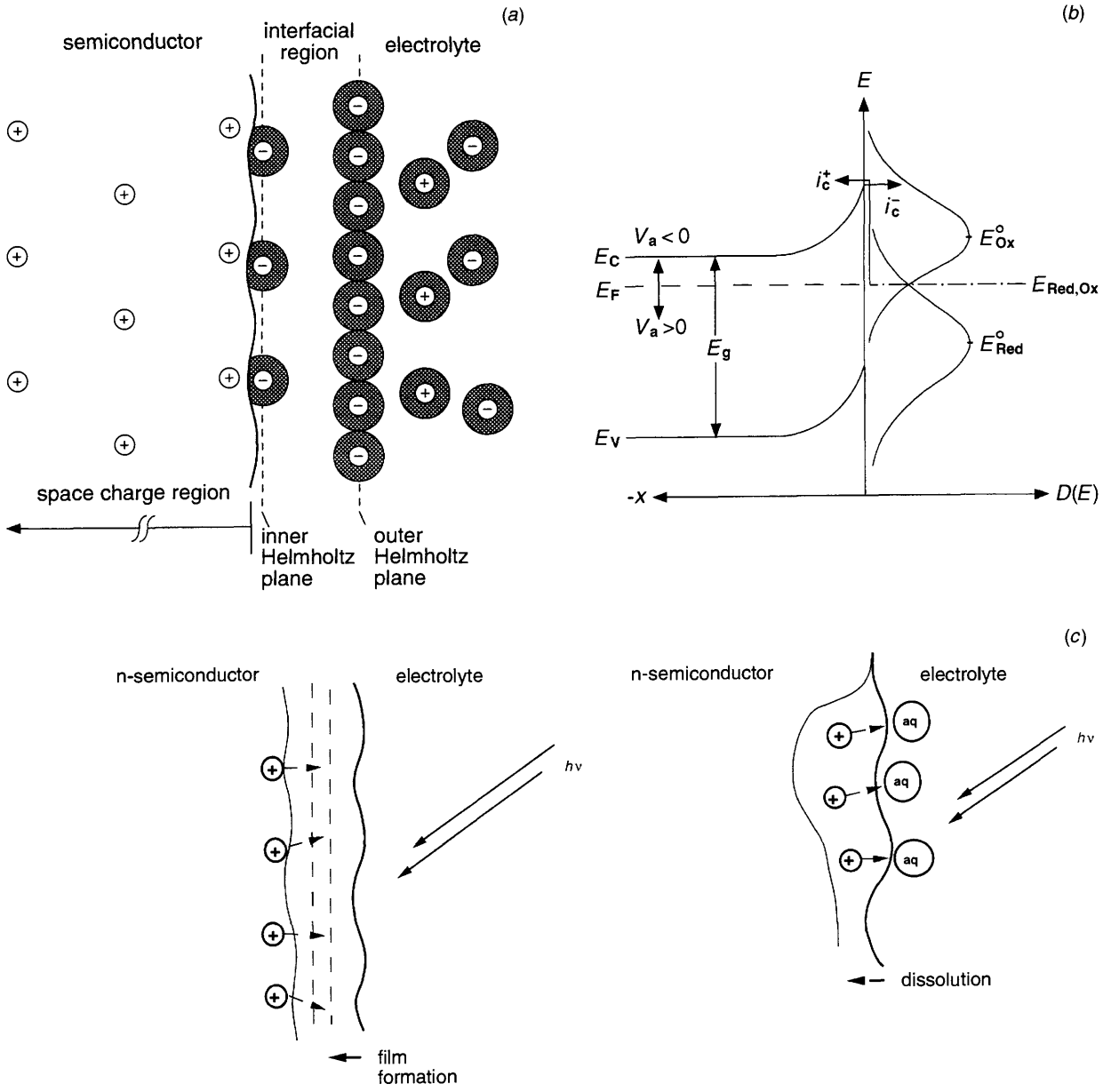

Fig. 2 Schematic illustration of processes at the semiconductor electrolyte interface; (*a*) charge distribution, (*b*) energetic scheme for charge transfer processes, (*c*) photocorrosion with insoluble film formation or semiconductor dissolution (see also text)

enough to result in a partial removal of the solvation shell as indicated in Fig. 2(*a*) by the semicircles. As a consequence the position of the band edges can be altered compared to the so-called flat band situation where no band bending (*i.e.* electrical field) exists in the semiconductor. In the ideal case (absence of surface states, specific adsorption and corrosion reactions) the flatband potential and the pzc should coincide.

Fig. 2(*b*) shows the charge transfer properties at the semiconductor–electrolyte junction. Depicted are redox reactions between electrons from the semiconductor conduction band and rechargeable species in the electrolyte [eqn. (2)].

$$Fe^{3+}_{aq} + e^{-}_{CB} \Leftrightarrow Fe^{2+}_{aq} \quad (2)$$

In this case, the electron which is transferred in a tunnel process according to[18] eqn. (3) (ν frequency factor, κ

$$k_{i\rightarrow f} = \int_{-\infty}^{\infty} \upsilon(E)\kappa(E_i = E_f)D_o(E_i)D_u(E_f)dE \text{ with } E_i = E_f \quad (3)$$

transition probability, D_o, D_u density of occupied and unoccupied states) stems from the semiconductor conduction band. The expressions for cathodic current flow are given by $i = qk_{i\rightarrow f}n_s$ (0) ($i_c = i_c^+ - i_c^-$) with:

$$i_c^-(V_a) = qk_c^-\kappa'(E_c)C_{ox}W_{ox}(E_c)n_S(0, V_a) \quad (4)$$

Since the charge transfer occurs in a narrow energy interval above and below the band edges, the integration with energy [eqn. (3)] is not necessary to a good approximation; $W_{red,ox}$ describes the thermal distribution function for electronic states in the redox electrolyte with gaussian character;[18] $n_S(0)$ is the electron concentration at the surface in the conduction band without applied voltage and C_{ox} the concentration of the oxidized species in solution. The voltage dependence at the semiconductor–electrolyte junction is given by the dependence of n_S (x = 0, V_a) (V_a, applied voltage). With the usual approximations,[19] this change is given by a Boltzmann term and the current–voltage curve for an n-type semiconductor depicted here is given by eqn. (5).

$$i_c(V_a) = i_{c,o}[\exp(-qV_a/kT)] \quad (5)$$

This is the diode equation known from solid state physics, except for the term $i_{c,o}$ which is different from the reverse saturation current in semiconductor diodes, eqn. (6).

$$\begin{aligned} i_{c,o} &= qk_c^-\kappa'(E_c)C_{ox}W_{ox}(E_c)n_S(x = 0, V_a = 0) \\ &= qk_c^+\kappa'(E_c)C_{Red}W_{Red}(E_c)N_c \end{aligned} \quad (6)$$

Here N_c is the effective density of states at the bottom of the conduction band. Finally, Fig. 2(*c*) shows the surface changes resulting from the interaction of electrons and holes with the semiconductor surface and the solution. For the case of photocorrosion[20] for instance, the formation of a passivation layer occurs if the product of the corrosion process is insoluble in the respective electrolyte. An example is shown in eqn. (7).

$$\text{n-CdS} + 2h^+_{VB}(h\nu) \rightarrow Cd^{2+}_{aq} + S^o_{film} \quad (7)$$

In this case the light induced excess charges are the holes from the valence band of n-type cadmium sulfide. The process results in the formation of soluble Cd^{2+} ions and an insoluble sulfur film which finally passivates the surface, inhibiting further charge transfer (current flow). It should be noted that the energetics of reaction (7) are also influenced by the intermediate step, *i.e.* the formation of Cd^+ and S^- on the surface.

In the case that the corrosion product is soluble, as for example for GaAs in aqueous solution, the semiconductor dissolves according to eqn. (8).

$$GaAs + 6h^+(h\nu) + aq \rightarrow Ga^{3+}_{aq} + AsO^{3-}_{3aq} + 6H^+_{aq} \quad (8)$$

The difference between photooxidation rate and dissolution rate determines whether a residual partly oxidized layer remains if the sample is removed from the solution or the light switched off since partly oxidized surfaces might not dissolve as well as fully oxidized ones (see above). An intermediate case in which current still flows in the presence of a thin interfacial film is found in the electropolishing of semiconductors. Here, a dynamic equilibrium exists between film formation rate and etch rate at a fixed film thickness and the electrical field at the electrolyte contact tends to smooth the surface since the carriers are following the trajectories of the field.

3 Selected surface analysis methods

In this section, a selection of experimental methods for analysing the semiconductor surface during (*in situ*) and after electrochemical treatment (*ex situ*) will be presented. The selection is made on the basis of the corresponding results, which will be presented and discussed subsequently.

3.1 Combined electrochemistry–UHV surface analysis system

The system shown in Fig. 3 is designed to allow the standard UHV surface analysis characterization directly after interrupting or terminating the electrochemical process without contact with ambient air. Therefore, a specifically constructed (photo)electrochemistry chamber is attached to a commercial surface analysis system.[6] This electrochemistry chamber is shown in detail in Fig. 3(*a*). Its main features are: (*i*) permanent flow of high purity dry N_2 gas, the use of O_2 free N_2-purged ultrapure water (Millipore), the use of highest available purity chemicals (ultrapure or reagent grade) for preparing the solutions; (*ii*) the semiconductor sample is mounted on a stub for direct transfer into the UHV preparation chamber and the respective electrolyte is supplied *via* a glass rod (L) which can also be used as light-guide for photoelectrochemical experiments; (*iii*) a cylindrical Pt electrode and a Luggin capillary are used as counter and reference electrode, respectively; (*iv*) for interruption of the experiment, the electrolyte solution can be removed by jet-blowing with N_2. This has the advantage of fast interruption (under potential, for instance) and since hydrocarbons tend to reside on the surface of water droplets, relatively low contamination of the semiconductor surface is expected; (*v*) after removal of the electrolyte, the semiconductor surface is thoroughly rinsed and dried in an N_2 stream. Nevertheless, it should be noted that this rinsing and drying procedure can influence the surface at the microscopic level investigated here. Species which are bound strongly enough to withstand rinsing and which are not easily dissolved in water will remain on the surface. Also, the drying procedure as well as the following outgassing in the preparation chamber of the UHV-system will result in a reduction of water and weakly bound hydroxy groups on the surface; (*vi*) finally the sample is transferred from the preparation chamber to the analysis chamber if the pressure in the former reaches values below 10^{-9} hp.

It turns out that this system and the procedure result in hydrocarbon contamination values after current flow in the electrochemical cell of *ca.* 0.15 monolayers. Consequently, all the established surface analysis methods can be applied, such as ultraviolet photoelectron spectroscopy (UPS), X-ray photoelectron spectroscopy (XPS), high resolution electron energy loss spectroscopy (HREELS) and low energy electron diffraction (LEED], for instance. The results of a UPS and an HREELS experiment on electrochemically hydrogenated silicon will be shown in Section 4.

3.2 *In situ* Fourier transform infrared spectroscopy

This method allows the measurement of interfacial changes during current flow by analysis of the vibrational losses from species formed in the electrochemical process. In the case of Si, which is presented here, a (111)-orientated single crystal is used in the attenuated total reflection–multiple internal reflection (ATR–MIR) mode (Fig. 4): the IR probe light enters the crystal

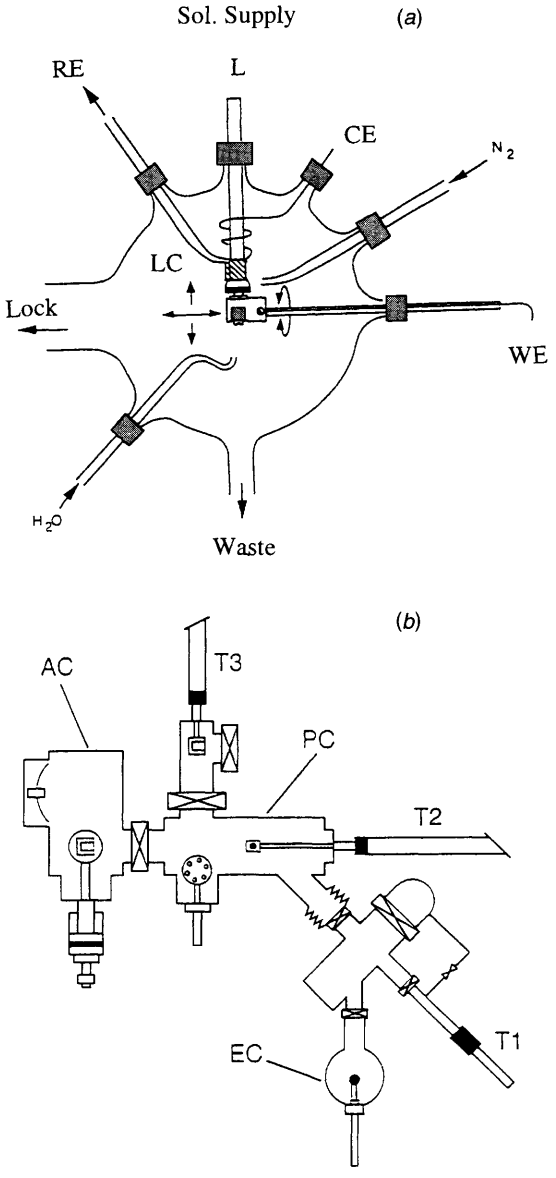

Fig. 3 Combined electrochemistry–UHV system for *ex situ* surface analysis; (*a*) details of the electrochemical vessel, L light guide and solution supply, CE counter electrode, WE working electrode, RE reference electrode, LC Luggin capillary (see text); (*b*) overview of the integrated EC–UHV system; PC preparation chamber, AC analysis chamber, T1, T2, T3 transfer rod, EC electrochemistry chamber

such that multiple total reflections occur at the silicon–electrolyte interface, the multiplicity of the reflections depending on the angle of incidence and the thickness of the crystal. Since the IR light does not have to penetrate the electrolyte solution, reflection losses due to Si–H and Si–O vibrations can be measured. The vibrations are excited by the evanescent wave directed parallel to the surface normal of the ATR crystal. Because of multiphonon absorption in the wavenumber region where the signal from the asymmetric Si–O stretching mode is expected, a particularly designed electrochemical cell with a Si crystal of drastically reduced size and thickness was used to minimize the optical path length to 11 mm in the material. Hence the Si–H stretching mode, analysed with a large (7 cm^2) crystal (as shown in Fig. 4) and the Si–O stretching mode become experimentally accessible. The Si–F vibration, however, lies outside our experimental range. The measuring cells are completed by a Pt counter electrode and a Ag/AgCl reference electrode as shown in Fig. 4.

3.3 *In situ* Electrochemistry–atomic force microscopy

Since the changes at semiconductor surfaces often result in the formation of films which either are passivating or less conductive than the substrate material, the microtopographic analysis is difficult to perform using standard scanning tunnelling microscopy.[21] In addition, the presence of the electrolyte and the problematic distinction between Faradaic and tunnelling currents makes this method less suitable. Instead, the scanning probe microscopy based on attractive and repulsive mechanical forces in the atomic region appears very well suited: insulating layers can be imaged and in addition the imaging process is not complicated by electronic processes. It allows a comparably accurate mapping of the surface microtopography, provided that the height changes compared to the width of flat regions are not too large. Otherwise, one would also have to take into account the finite size and shape of the imaging needle.

The AFM method uses the fact that the probing needle, once it is in attractive contact with the sample, is moving with the sample structure when measuring in the so-called constant force mode (Fig. 5). The needle deviation is translated *via* a laser beam deflection system on a photodiode array allowing accurate height measurements (after calibration with well known steps on mica, for instance). Because of the laser light, the investigation of n-type Si appears problematic. In this case the light produces holes as excess carriers which can undesirably oxidize the surface. Consequently, anodic reactions of Si investigated by EC–AFM were performed with p-Si where the light-induced excess carriers are electrons and anodic polarization results in a deflection of electrons away from the interface.

4 Selected results and discussion

4.1 Fundamental electrochemical observations

The (photo)electrochemistry of Si in aqueous fluoride-containing solutions is characterized by a series of surprising features. Among them is the observation of quantum yield multiplication,[22] the occurrence of a dark current transient on formerly oxidized Si surfaces,[23] the formation of ultrathin nanoporous Si in dilute ammonium fluoride solutions at potentials positive from flatband,[24] an electropolishing regime and current oscillations.

Fig. 6 shows a typical photocurrent–voltage curve (*a*) and a dark current transient (*b*) obtained on n-Si(111). The i_{Ph}–V characteristic [Fig. 6(*a*)] exhibits two maxima and for $V > 4$ V, photocurrent oscillations set in. In the region between flatband and the first maximum, porous Si is formed, as evidenced by a series of *in situ* FTIR and high resolution scanning electron microscopy experiments.[25] At larger anodic potentials, oxide formation and electropolishing of the surface followed by the formation of thicker oxides and current oscillations also take place as indicated in Fig. 6. The dark current displayed in Fig. 6(*b*) is always observed when an oxidized Si sample is exposed to F^- containing acidic solution. Following electroless etching of SiO_2 according to eqn. (9), the current rises when

$$SiO_2 + 6HF + aq \rightarrow SiF_6^{2-} + 2H_2O + 2H^+_{aq}$$
$$SiO_2 + 3HF^-_{2aq} + aq \rightarrow SiF_6^{2-} + H_2O + OH^-_{aq} \qquad (9)$$

the etch front reaches the silicon oxide–silicon interface thus making contact between the Si and the electrolyte. *Ex situ* XPS and UPS analyses using the system described in Section 3.1 (see also Fig. 3) have shown that the surface undergoes a transformation from oxidic coverage, enrichment of F^- at the surface around the dark current (i_D) maximum and increasing hydrogenation during the decay and levelling out of i_D.[26] Several electrochemical methods to prepare H-terminated Si(111), Si(113)[27] and Si(100) surfaces have been developed. Best results with respect to smoothness of the surface and high electronic quality were obtained by a two-step procedure in which the oxide etching is made at pH 4.0 and residual oxidic

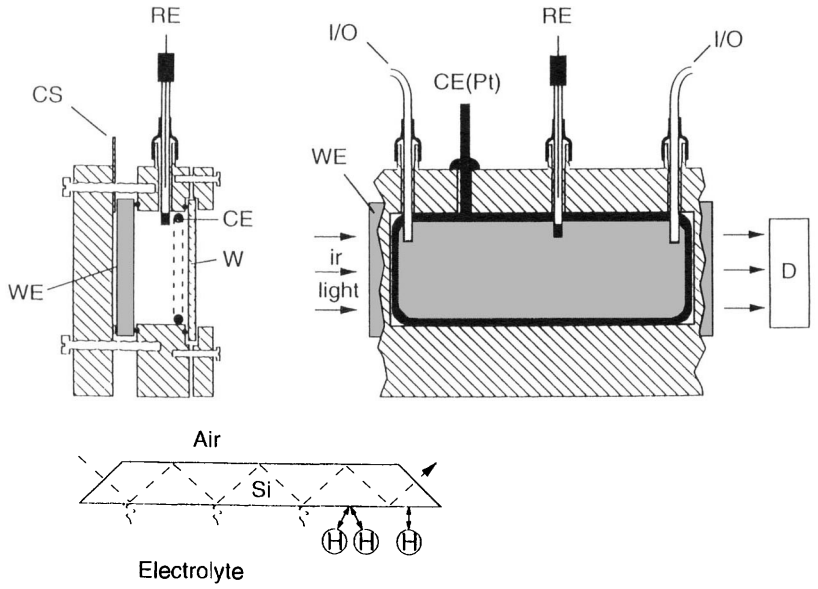

Fig. 4 Experimental arrangement for FTIR measurements in the ATR–MIR configuration; W window, CS spacer, I/O in and outlet, D detector, CE, WE, RE, as in caption of Fig. 3

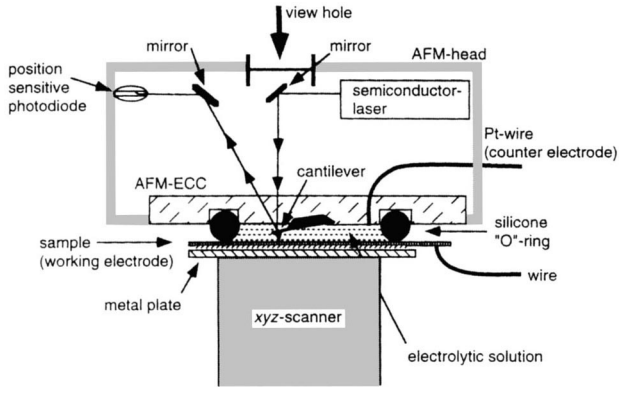

Fig. 5 Experimental arrangement for *in situ* electrochemistry–AFM measurements; see indications in the figure

traces are then removed by subsequent etching in a solution with pH 4.9, where the oxide etch rate[28] [eqn. (10)], is very small.

$$k_e = a[HF] + b[HF_2^-] + C \qquad (10)$$

Another procedure uses sustained photocurrent oscillations at large anodic potentials [+6 V (SCE)] followed by a change in potential to +0.5 V (SCE; standard calomel electrode) in the dark where the oxide present during oscillations is removed during the dark current transient. The latter method allows the preparation of surfaces with very high electronic quality (see below Section 4).

4.2 The hydrogenated Si(111)-H (1 × 1) surface

Using the combined electrochemistry–UHV surface analysis system (Fig. 3), the surface of Si(111) has been analysed by high resolution energy loss spectroscopy (HREELS).[15] This technique allows the detection of vibrational losses of primary low energy electrons impinging on the surface, measured in specular reflection geometry. The result of such an experiment in which the surface has been prepared by the aforementioned two-step electrochemical procedure is given in Fig. 7. The Si–H bending mode and the Si–H stretching mode are very pronounced (78 and 257 meV, respectively) although the excitation cross section is comparably low, revealing the high quality of the surface. Additional vibrations occur due to phonons or due to oxidic and hydroxidic remnants as indicated in Fig. 7. Small

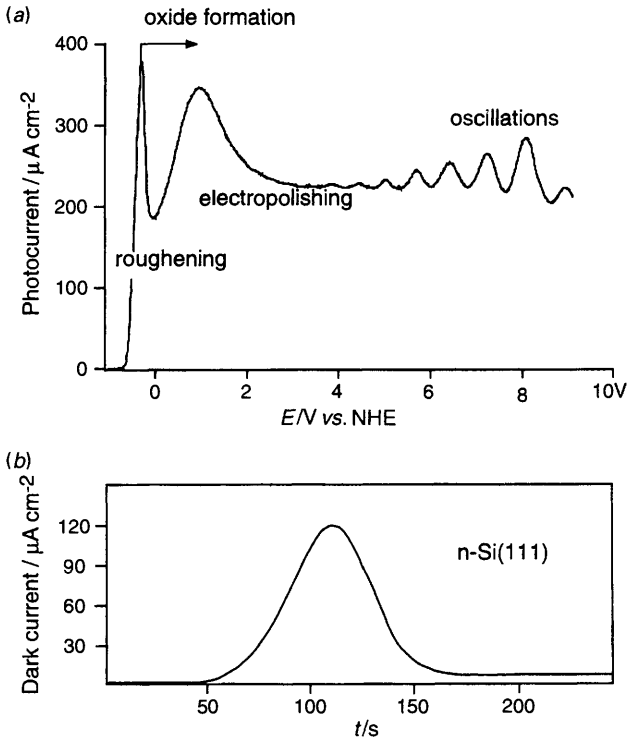

Fig. 6 Current characteristics of Si(111) in aqueous ammonium fluoride solution; (*a*) photocurrent–voltage curve pH 4.0, 0.1 M NH_4F, light intensity 20 mW cm^{-2} (tungsten–iodine lamp); (*b*) dark current *versus* time; pH 0.1 M NH_4F (NHE = normal hydrogen electrode)

parts of the surface are covered by OH groups and some oxygen is found in the Si backbonds.

The electronic band structure of ideally H-terminated Si(111) surfaces has been calculated theoretically[29] and the data are shown in Fig. 8 together with a result from UPS measurements with variation of the polar angle of the emitted electrons. In Fig. 8(*a*) the electronic bands along symmetry lines of the surface Brillouin zone (BZ) are plotted. It can be seen that gaps in the projected bulk band structure exist, for instance along $\bar{\Gamma} - \bar{K}$, $\bar{\Gamma} - \bar{M}$ and $\bar{K} - \bar{M}$, near the outer part of the surface BZ at energies between 4 and 7 eV below the valence band edge [zero energy on the scale of Fig. 8(*a*)]. The hydrogenation of the

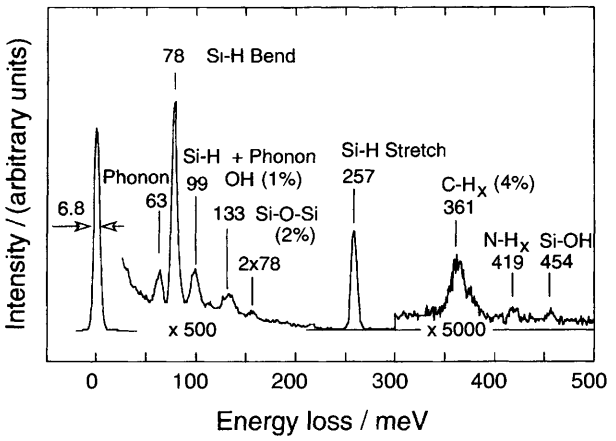

Fig. 7 High resolution electron energy loss spectrum of Si(111) obtained by removal after the decay of the dark current at pH 4.0, subsequent immersion into a solution of 0.1 M NH_4F with pH 4.9 and final removal after levelling out of the residual dark current (two step procedure); primary electron energy 6 eV, energy resolution 4 meV, background pressure 1×10^{-10} hp

surface leads to additional electronic states which partly overlap with the bulk band structure (surface resonances) and partly lie within the forbidden regions. The latter surface states due to the hydrogenation would be expected at tilt angles of *ca.* 20° to 30° of the surface normal of the Si sample towards the electron analyser at energies below the valence band edge of 3.8 eV [small gap in Fig. 8(*a*)] and 4.5 eV (large gap).

Fig. 8(*b*) shows two photoelectron spectra of a Si surface treated by the two-step procedure for the dark current: at $\theta = 0°$, the surface normal points towards the electron analyser and the well known band structure features of Si due to emission from 3p levels (valence band top) and lower lying 3s levels are observed. At a 25° tilt angle, however, the spectrum is drastically changed. The emission from the Si 3p level at −1.3 eV is quenched according to the dispersion of the initial state towards $\bar{K}$ ($\bar{\Gamma}$ corresponds to normal emission) which is lowered to *ca.* −2 eV at $\theta = 25°$. Furthermore, a dispersion of the maximum at −7 eV (Si 3s, 3p) towards lower binding energy is noted, in accordance with the calculated band structure (lower band at −7.8 eV at $\bar{\Gamma}$). The most prominent feature, however, is the occurrence of a maximum at $E_B = -4.5$ eV which can clearly be attributed to the Si–H surface band in excellent agreement with the theory. The expected small signal at −3.8 eV cannot be observed at this tilt angle.

The process of surface hydrogenation can also be monitored *in situ* by FTIR. In this case, two surface treatments are compared: the first electropolishing treatment, keeping the sample for 15 min at +1.6 V (SCE) at a photocurrent density of $i_{Ph} = 400\ \mu A\ cm^{-2}$; this treatment is known to produce smooth surfaces with very low density of interface states. The second procedure consists of the aforementioned combined photocurrent oscillation and dark current decay. Fig. 9 shows the FTIR signals for electropolishing (curve *b*) and for the two step procedure involving oscillations (curve *a*) with reference to the Si–H free surface (oxidized Si) in the wavenumber region of the Si–H and $Si{=}H_2$ stretching modes. A pronounced signal at *ca.* 2080 cm^{-1} (Si–H) and 2120 cm^{-1} ($Si{=}H_2$) is found for both treatments indicating hydrogenation of the surface. From the difference spectrum (*c*) obtained by subtracting spectra (*b*) − (*a*) one sees a remaining signal which can be attributed to the $Si{=}H_2$ stretching mode. Since two H atoms are exposed at steps in the direction of a (111) surface, the difference spectrum (*c*) shows that the combined oscillation procedure results in a reduced density of such steps compared to electropolishing, hence the surface after treatment (*a*) is smoother than after treatment (*b*).

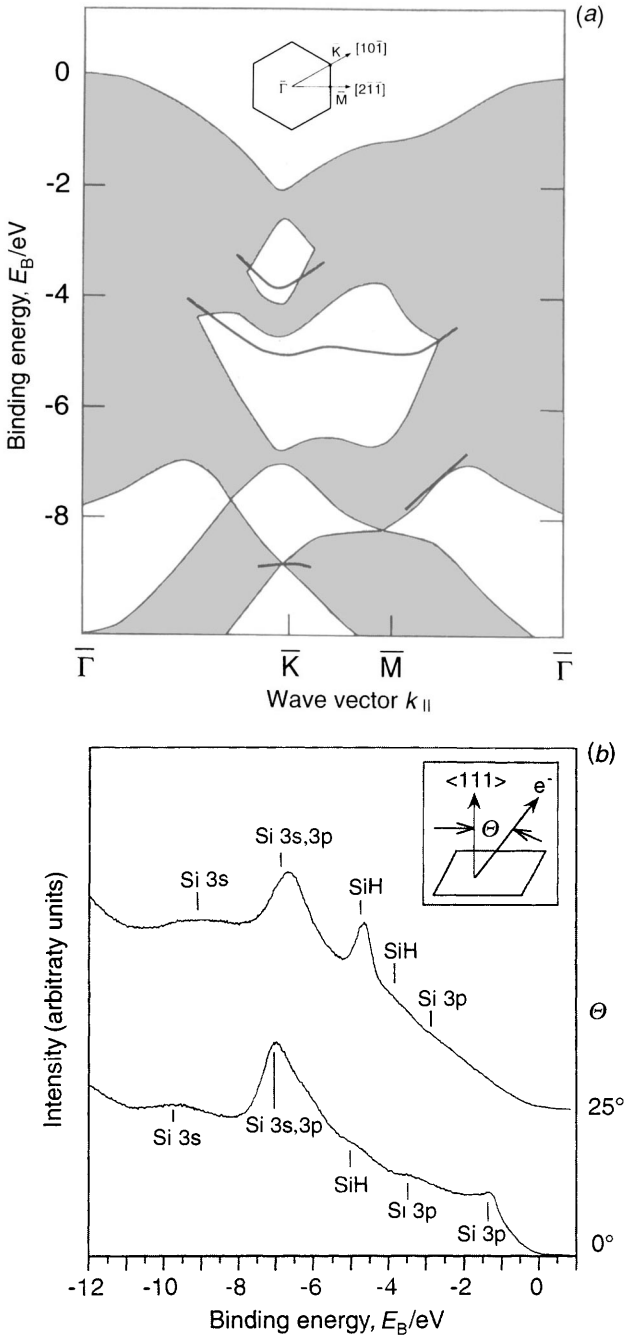

Fig. 8 Photoelectron spectroscopy on Si(111) treated by the electrochemical two step procedure; (*a*) surface band structure calculation for hydrogen terminated Si(111); (*b*) photoelectron spectra obtained for normal emission ($\theta = 0°$) and for a tilt angle θ of 25° (see text); detector acceptance angle ±15°

4.3 *In situ* analysis of dynamic processes during current oscillations

The dependence of the oscillation period on solution composition allows the adjustment of oscillations which are slow enough to be followed by *in situ* techniques such as FTIR, EC–AFM and microwave reflectivity, for instance. In the following the changes of the Si–O vibrational absorption during photocurrent oscillations and of the outer oxide topography will be investigated. With a modified ATR–MIR configuration using a miniaturized cell, the asymmetric Si–O stretching vibration in the wavenumber region between 980 cm^{-1} and 1260 cm^{-1} could be monitored simultaneously with the current oscillation.

In a different experiment, the topography at the oxide–electrolyte interface was monitored by *in situ* AFM simultaneous with the current oscillation at p–Si. The roughness was determined from line scans across the sample according to eqn. (11), where the surface topography is described by the

$$R_a = \int_0^{L_x}\int_0^{L_y} |f(x,y)|dxdy \qquad (11)$$

function $f(x, y)$ and L_y, L_x are the lengths of the line scans. The two sets of experiments (photocurrent oscillation, Si–O signal and current oscillation, roughness) were made under slightly different experimental conditions: the former experiment was performed in 0.1 M NaF on n-Si(111) at pH 4.0 with a period of 95 s. The AFM experiment was made in 0.1 M NH_4F at pH 4.2 (to increase the period since the recording period is 5 s with AFM) on p-Si(111). The very characteristic behaviour of each experiment is condensed into Fig. 10 by adjusting the timescale accordingly and plotting the photocurrent, the roughness and the Si–O absorption *vs.* time. It is found that the roughness is largest in the increasing region of the current and drops already when the photocurrent reaches its maximum value. The Si–O signal varies by more than ±20% (*ca.* ± 5 monolayers under these experimental conditions) and is minimal at the time when the roughness is largest. These data cannot easily be interpreted and I will merely describe the findings: the maxima in the photocurrent are confined to a smaller time region than the more extended minima. This fits with the observation that the Si–O signal exhibits two slopes. The formation (increasing Si–O signal) appears to be faster than the chemical dissolution (smaller slope). Since the maximum oxide thickness is reached at the decreasing branch of the photocurrent, passivation is good and the oxide etches chemically obviously resulting in a smoothing of the outer oxide parts. Around the minimum oxide thickness the roughness reaches its maximum indicating that a rough surface of the inner part of the oxide has been reached by the etch front. With increasing current the then growing oxide at the silicon–silicon oxide interface results in a smoothing of the silicon oxide at the electrolyte interface due to simultaneous etching. Further investigations on the corresponding microwave reflectivity which allows us to distinguish between charge transfer and surface recombination losses are presently being performed. In addition a spatial coupling of the oscillations *via* the electrolyte has been found but it is too early yet to arrive at conclusive model descriptions.

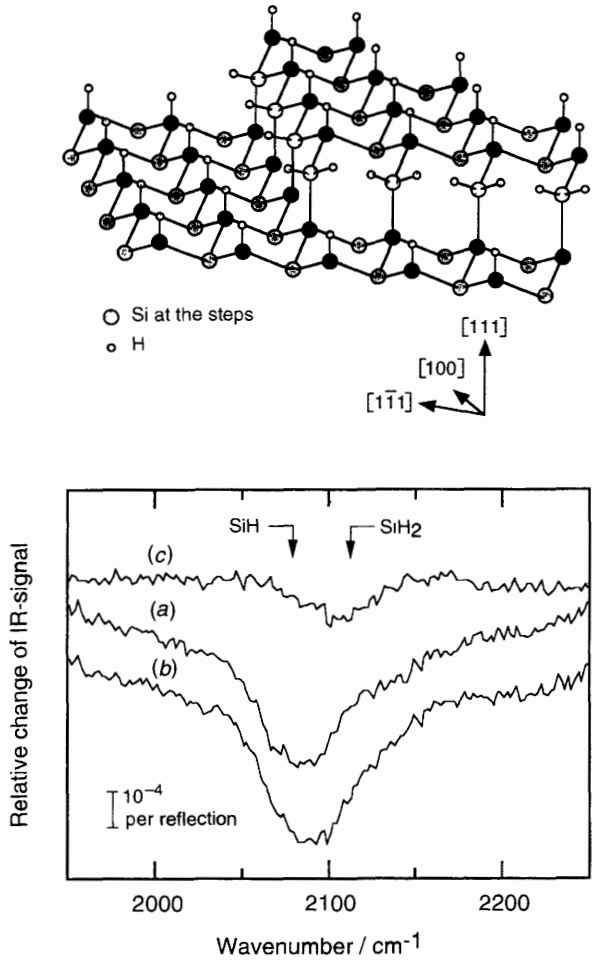

Fig. 9 FTIR spectra on Si(111) for different surface conditioning; (*a*) after photocurrent oscillations at +6 V (SCE); (*b*) after electropolishing (see text); (*c*) difference spectrum (*b*) − (*a*); solution 1M NaF pH 4.0

5 Synopsis

The modern surface analysis methods can be very well applied for the investigation of surface changes which occur during electrochemical processing of semiconductors. Several difficulties, however, have to be kept in mind: the analysis using *ex situ* methods (UPS, XPS, HREELS and LEED) involves three steps which are not uncritical. First, the sample has to be removed from the electrochemical cell. Whether this is done under applied external potential or at the rest potential can already alter the surface condition. The second step involves the transfer from the electrochemical environment to, for instance, a UHV preparation chamber. It is very important that contamination from the respective laboratory ambient is suppressed as much as possible. The rinsing and drying procedure after removal from the cell also belongs to this transfer step and might lead to surface alterations due to the removal of less strongly bound adsorbates or to dissolution of species in the ultrapure oxygen free rinsing water. On the other hand, precipitates formed upon removal from the cell can be dissolved. The third step is the outgassing of the sample in the preparation chamber of a UHV system. Here, weakly bound water and hydroxy groups can evaporate leaving a surface with an eventually more open structure and a formerly hydrophilic surface can change to hydrophobic. The application of such techniques to hitherto unknown surface modifications is important and worthwhile even if not all the effects introduced during the three transfer steps are well known, but it should be

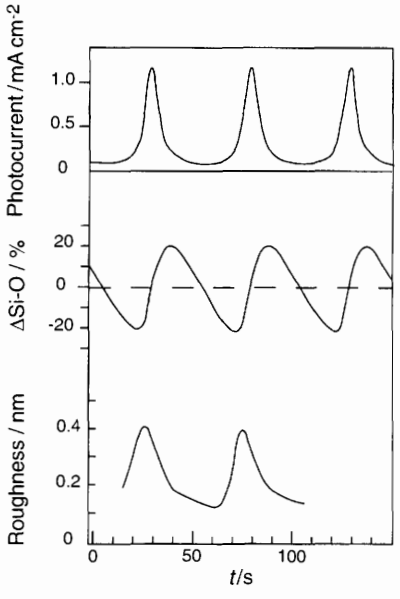

Fig. 10 Comparison of the temporal evolution of current, integrated Si–O signal obtained from FTIR and roughness parameter during current oscillations on Si(111) (see text)

stressed that the uncertainties of the procedure are kept in mind when interpreting the obtained data. For the hydrogen terminated hydrophobic Si(111) surface, these difficulties are marginal and we can make use of the HREELS experiment, for instance. This technique allows us to identify almost all the species present on and even below the topmost atomic layer with high resolution in the submonolayer range.

The *in situ* methods give a more realistic description of the surface changes but since they include the analysis of water and hydroxy groups into surface films, it is difficult to judge whether the *in situ* monitored surface condition is stable for a subsequent process in a technology line. In addition, if one considers the example of the FTIR method, only Si–H and Si–O species can be monitored since Si–F is outside the experimentally accessible range in the ATR–MIR configuration. Therefore, the information gained here is more direct but less general compared to an HREELS experiment.

The *in situ* AFM method can give very important information on topographical changes not otherwise obtainable. It should be noted, though, that the images contain a temporal development during the scanning procedure and that the influence of illumination by the laser deflection system has to be excluded. It is this author's opinion that due to the complexity of the sample handling procedures reliable results can only be obtained by a combination of *ex situ* and *in situ* techniques, particularly if the introduced surface modification is made for specific applications in semiconductor devices such as solar cells and transistors.

6 Acknowledgements

I am indebted for their important contributions and many enlightening and rewarding discussions to the following persons: Professor Karl Jacobi, Dr Markus Gruyter (Fritz-Haber-Institut der Max-Planck-Gesellschaft) and Dr Thomas Bitzer (International Surface Science Centre, Liverpool) for the HREELS investigation; Dr Jörg Rappich, Mr Stefan Rauscher (Hahn-Meitner-Institut Berlin) for the FTIR experiments; Dr Helmut Jungblut, Mr Oliver Nast (Hahn-Meitner-Institut) for the EC–AFM research, Mr Stefan Rauscher for the UPS investigation and Ms Wiebke Frandsen for drawing the figures.

References

1 L. M. Peter, D. J. Blackwood and S. Pons, *Phys. Rev. Lett.*, 1988, **62**, 308.
2 R. A. Venkateswara, F. Ozanam and J. N. Chazalviel, *J. Electrochem. Soc.*, 1991, **138**, 153.
3 H. J. Lewerenz and T. Bitzer, *J. Electrochem. Soc.*, 1992, **139**, L21.
4 J. Stumper, R. Greef and L. M. Peter, *J. Electroanal. Chem.*, 1991, **310**, 445.
5 H. J. Lewerenz, T. Bitzer, M. Gruyters and K. Jacobi, *J. Electrochem. Soc.*, 1993, **140**, L44.
6 T. Bitzer and H. J. Lewerenz, *Surf. Sci.*, 1992, **269/270**, 886.
7 D. J. Blackwood, A. Borazio, R. Greef, L. M. Peter and J. Stumper, *Electrochim. Acta*, 1992, **37**, 889.
8 H. J. Lewerenz and H. Jungblut, in *Semiconductor Micromachining*, vol. I (*Fundamentals*), ed. S. A. Campbell and H. J. Lewerenz, Wiley, London, 1997, ch. 3.
9 J. Rappich and H. J. Lewerenz, *Electrochim. Acta*, 1996, **41**, 675.
10 H. J. Lewerenz, D. E. Aspnes, B. Miller, D. L. Malm and A. Heller, *J. Am. Chem. Soc.*, 1982, **104**, 3325.
11 S. Menezes, H. J. Lewerenz and K. J. Bachmann, *Nature*, 1983, **305**, 615.
12 D. Mahalu, L. Margulis, A. Wold and R. Tenne, *Phys. Rev. B*, 1992, **45**, 1943.
13 A. Heller, *Acc. Chem. Res.*, 1981, **14**, 154 and references therein.
14 H. J. Lewerenz, M. Lübke, K. J. Bachmann and S. Menezes, *Appl. Phys. Lett.*, 1981, **39**, 798.
15 G. L. Schnabel and P. F. Schmidt, *J. Electrochem. Soc.*, 1976, **123**, 310C.
16 H.-M. Kühne and H. Tributsch, *J. Electroanal. Chem.*, 1986, **201**, 263.
17 C. H. Hamann and W. Vielstich, *Electrochemie I*, Verlag Chemie, Weinheim, 1975.
18 H. Gerischer, *J. Electrochem. Soc.*, 1984, **131**, 2452.
19 H. J. Lewerenz and H. Jungblut, *Photovoltaik, Grundlagen und Anwendungen*, Springer Verlag, Heidelberg, Berlin, New York, 1995.
20 H. Gerischer, in *Semiconductor Liquid Junction Solar Cells*, The Electrochemical Society, Proc. vol. 77–3, ed. A. Heller 1977, ch. 1.
21 S. Rauscher, T. Dittrich, M. Aggour, J. Rappich, H. Flietner and H. J. Lewerenz, *Appl. Phys. Lett.*, 1995, **66**, 3018.
22 H. J. Lewerenz, J. Stumper and L. M. Peter, *Phys. Rev. Lett.*, 1988, **61**, 1989.
23 M. Matsumara and S. R. Morrison, *J. Electroanal. Chem.*, 1983, **147**, 157.
24 J. Rappich, H. Jungblut, M. Aggour and H. J. Lewerenz, *J. Electrochem. Soc.*, 1994, **141**, L99.
25 T. Dittrich, S. Rauscher, V. Yu. Timoshenko, J. Rappich, I. Sieber, H. Flietner and H. J. Lewerenz, *Appl. Phys. Lett.*, 1995, **67**, 1134.
26 J. Rappich and H. J. Lewerenz, *J. Electrochem. Soc.*, 1995, **142**, 1233.
27 K. Jacobi, M. Gruyters, P. Geng, T.Bitzer, M. Aggour, S. Rauscher and H. J. Lewerenz, *Phys. Rev. B*, 1995, **51**, 5437.
28 J. S. Judge, *J. Electrochem. Soc.*, 1971, **118**, 1772.
29 K. C. Pandey, *Phys. Rev. B*, 1976, **14**, 1557.

Received, 24th March 1997
Accepted, 10th April 1997